Proceedings of the Canadian Society for Mechanical Engineering International Congress 2022
CSME Congress 2022
June 5-8, 2022, Edmonton, AB, Canada

Process Parameters Optimisation for FSW of Al/Stainless Lap Joint

Lyne St-Georges[1], François Nadeau[2], Francis Tremblay[1]
[1]Applied Sciences, Université du Québec à Chicoutimi, Saguenay, Canada
[2] Aluminium Technology Center (NRC), Saguenay, Canada

Abstract—The necessity of reducing fuel consumption and the increasing demands for lightweight vehicles have motivated the use of multi-material combinations. Dissimilar metals have been progressively introduced in different locations to optimize mechanical performance and strength-to-weight ratio. These new combinations of metals need to be joined, which presents a major challenge in conventional fusion welding. Since FSW does not involve bulk melting of the components, it is among the most convenient welding techniques for joining dissimilar materials. In this investigation, process parameters are optimized to produce friction stir lap welds between an aluminum alloy AA5083-H19 and a stainless steel 201LN ¼ hard. For the welding procedure, a WC-25Co welding tool is used. The tool is rotated and penetrated through the aluminum alloy located on the top of the assembly. Key parameters considered to obtain an optimal process window include rotation speed, travel speed, surface and internal defects, lateral force and tool degradation. Microstructural characterization was done by optical and scanning electron microscopy. Tensile lap shear tests were conducted for mechanical property evaluation. Joints produced exhibit good mechanical properties with a tensile shear strength up to 500 N/mm of weld. During the FSW, a significant degradation of the tool was observed due to the combination of high welding temperatures and high material flow stress at the end of the pin tool, where the tool is in contact with the stainless steel. Tool wear was investigated by using 3D digital profilometry scans. Abrasion and adhesion were found to be the most dominant causes of wear.

Keywords-friction stir welding of dissimilar materials; lap joint; process optimization; tool wear

I. INTRODUCTION

Friction stir welding (FSW) is a solid-state welding process, patented in UK in 1991 by The Welding Institute (TWI). The process, illustrated in Fig. 1, uses a non-consumable tool to join two facing surfaces without melting. The FSW tool is specially designed with a pin and a shoulder. To produce a weld, the rotating tool is plunged in the material, until the shoulder touch the upper surface of the joint. The frictional heat produced at the tool material interface causes a plasticized zone to form around the tool. As the rotating tool moves along the joint line with a prescribed advancing speed, a consolidated solid-phase joint is formed. Due to the low energy input used, FSW creates high strength joints with reduced distortion. Being capable of handling variations inherent to high volume production, advantages of FSW also include improved process robustness and reduced production costs.

FSW has rapidly gained acceptance for the manufacturing of lightweight structures. The rising demands for improved fuel economy have driven the efforts for the development of innovative aluminum products for transportation vehicles and an increased utilization of aluminum. To date, FSW in the automotive industry has been mainly used for body-in-white applications. The majority of structures used in vehicle involve steel and the employment of lightweight materials in steel structures is of great interest. The use of combinations of steel and aluminum has been increasing in fabrication and many efforts to weld steel to aluminum alloys have been explored, including resistance spot welding (RSW) and arc welding processes (plasma-arc and Cold Metal Transfer®). Despite the differences in thermal and mechanical properties and materials flow, sound weld of Al to steel is obtained by FSW.

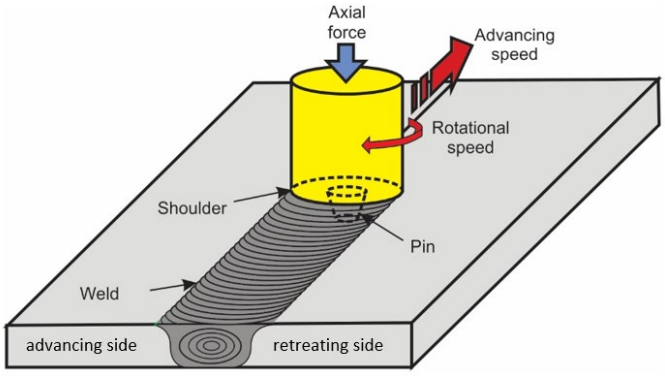

Figure 1. Illustration of FSW [1]

FSW shows a large advantage for dissimilar welding applications due to lower welding temperatures leading to significantly less intermetallic formation. For example, in the mass production of vehicles by Honda Motor Co. Ltd., a hybrid structure of aluminum and steel was produced by FSW in the sub-frame of its 2012 Accord model [2].

However, the welding of hard metals like stainless steel creates an extremely high stress region coupled with high temperatures (up to 1300 °C) which promotes FSW tool degradation. Friction Stir Welding of steel has been in development for over a decade, but only in recent years, the strength and wear characteristics of tool materials have improved sufficiently to promote new developments [3, 4]. Although the benefits of FSW to join aluminum to stainless steel are clear, the applications of FSW to join alloys with high melting temperature have been limited due to stringent demands on the tool. The FSW tool is subjected to severe stress and high temperatures particularly for the welding of hard alloys such as steels, which promotes tool degradation. For these materials, the commercial application of FSW is limited by the high cost and short life of the tools.

The joining of aluminum to steel or stainless steel can offer important weight savings in lightweight structures. For the automotive industry, replacing steel with aluminum promotes weight reduction without significant vehicle downsizing. This substitution allows for additional engine downsizing (along with turbos) to improve fuel economy without reducing performance. For example, a 10 % reduction in curb weight results typically in a 6 to 7% fuel economy improvement (including engine downsizing) [5]. Using FSW, hybrid structure of aluminum and steel has been successfully realized in the past and FSW opens up more opportunities to use aluminum to trim vehicle weight. According to automotive expert, it is expected to start seeing FSW everywhere in the automotive sphere. Although the process has been successfully demonstrated, further developments are needed to improve tool material technology, process control and to obtain more data on the performance of welds and tool degradation. Process economics for welding aluminum to stainless steel have also not been fully established and the robustness of the process needs further consideration. Typical applications include mass transportation vehicles such as railcar or bus components. These markets require high lifetime, which dictates the use of corrosion resistant steel grades as stainless steels. In this investigation, process parameters are optimized to produce friction stir lap weld between aluminum alloy AA5083-H19 and stainless steel 201LN ¼ hard. Due to its important impact on massive production of friction stir welded parts, particular attention is given on tool wear.

II. METHODOLOGY

Friction lap joint welds were made between 1.7 mm thick hot-stamped AA5083-H19 aluminum alloy and 2.3 mm thick 201LN ¼ hard stainless steel. The chemical composition of the metals used was measured by optical emission spectroscopy (OES) and is presented in Table I. Mechanical properties were obtained by tensile test following ASTM E8 procedure and are presented in Table II. These two materials were selected according to their potential in automotive and mass transportation applications. The aluminum alloy 5083-H19 has been developed to obtain, from a basic microstructure and a high degree of hardening (H19 temper) and fine grains after forming [6]. The SS201LN ¼ hard is an austenitic stainless steels with a good formability and corrosion resistance. It is a low cost alternative to conventional Cr-Ni austenitic stainless steels due to the replacement of nickel with a manganese content.

For welding, a tool made of WC-25% Co with a concave shoulder and a cylindrical pin with a convex tip was used, as depicted in Fig. 2. The total length of the pin was adjusted to obtain a 0.3 mm of penetration depth in the stainless steel in order to avoid rapid and detrimental wear. The dimensions of the welding tool are listed in Table III. During the welding, a tool inclination of 2.5° relatively to the vertical axis, in the welding direction, was used to minimize the amount of flash produced, based on previous work.

TABLE I. CHEMICAL COMPOSITION OF BASE METALS WELDED

Metal	Content (% mass)				
AA5083-H19	Si	Fe	Cu	Mn	
	0.052	0.089	0.028	0.865	
	Mg	Al	Other		
	4.72	94.00	Bal.		
SS201LN ¼ hard	C	Si	Mn	S	Ni
	0.034	0.445	6.979	0.002	4.547
	Cr	Cu	Co	Mo	Fe
	16.771	0.040	0.118	0.375	70.200

TABLE II. MECHANICAL PROPERTIES OF BASE METALS WELDED

Metal	Testing orient.	Specimen dimensions		Yield Stress (MPa)	Ult. stress (MPa)	El. at break (%)
		Thick. (mm)	*Width (mm)*			
AA 5083 SPF	Long.	1.74	12.75	149.6	301.1	23.8
	Trans.	1.73	12.76	148.1	292.0	24.2
SS 201LN	Long.	2.22	12.77	531.8	911.8	54.3
	Trans.	2.32	12.76	572.3	819.9	45.6

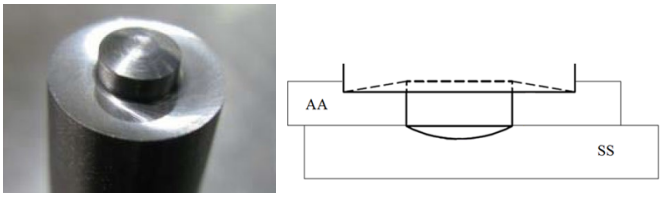

Figure 2. Global geometry of welding tool and assembly

TABLE III. WELDING TOOL DIMENSIONS

Pin		Shoulder	
Diameter Length conical part Length convex tip (plunged in SS)	5 mm 1.6 mm 0.6mm	Diameter	11 mm

Figure 3. MTS I-Stir PDS system used for welding, NRC Saguenay

For the welding procedure, the tool is rotated and penetrated through the aluminum alloy located on the top of the lap weld and the tool pin lightly plunged into the lower stainless steel part (see Fig. 2). Welds were produced on 300 mm coupons in force control, using a MTS I-Stir PDS system illustrated in Fig. 3. This system is equipped with load sensors: torque, axial, longitudinal and lateral forces are continuously monitored. To follow the temperature evolution during welding, a K-type thermocouple was inserted in the welding tool, centered at the base of the pin and connected to a telemetry system.

To optimise welding conditions, key parameters considered were the amount of flash produced, the presence of surface and internal defect and tool degradation. Microstructural characterization were done with optical and scanning electron microscopes. Finally, tensile lap shear tests were conducted for mechanical property evaluation. Tool wear measurements were done using 3D microtopography. A STIL system with a moving table and a fixed optic pencil with a precision of 1µm was used. Results were analyzed with Mountain maps ® software. To evaluate wear, the tip profile of the tool was recorded periodically, after specific weld length. Different techniques were investigated to characterize the wear but from a practical point of view, the pin length was identified as the most significant parameters. For a lap joint, the length of the pin must be sufficient to react with the lower part of the lap joint to induce a joint and must be controlled.

III. RESULTS

Preliminary bead on plate tests were performed to set initial welding boundaries. The welding speed was then varied from 0.3 to 1.25 m/min and rotational speed from 500 to 1500 RPM. Welding conditions producing small defects and good tensile lap shear resistance with low lateral force (lower than 16 kN) where selected to define the optimal process window. The lateral force applied by the welding equipment was considered for future massive automotive production, where welding robots used have limited capacity to apply lateral force. The presence of surface or internal defects was also considered as they can reduce fatigue life or produce higher corrosion rates. The welding conditions tested are reported in a Fig. 4, where typical defect and optimal process window are identified. In this figure, the optimal process window is delimited by the two dashed lines. Tensile lap shear test results are presented in Table IV. In this table, the conditions highlighted in grey exhibit severe internal volumetric defects and for the conditions highlighted in yellow, large lateral forces were recorded during welding. The maximum tensile shear resistance of 501.1N/mm of weld was obtained at 1.25 m/min and 750 RPM (weld. no. 12). However, this condition was not considered for the optimal process window, due to large lateral force measured on the welding tool, exceeding welding robot capacity.

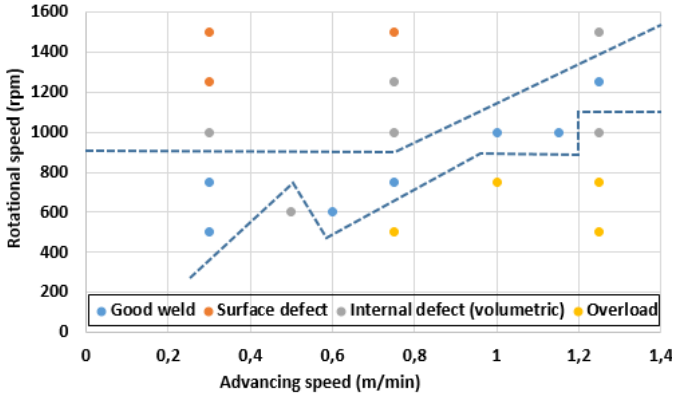

Figure 4. Optimal process window

TABLE IV. MECHANICAL RESISTANCE OF AA5083-H19/ SS201LN ¼ HARD LAP WELDS, OBTAINED FROM TENSILE LAP SHEAR TESTS

Weld no.	Ad. Speed (m/min)	Rot. Speed (RPM)	Resistance (N)	Resist./weld length (N/mm)
1	0,30	500	12463	485,9
2	0,30	750	11448	442
3	0,30	1000	10503	405,4
6	0,75	500	12233	471,4
7	0,75	750	12901	488
8	0,75	1000	11187	430,9
9	0,75	1250	10697	416,1
11	1,25	500	12302	474,4
12	1,25	750	12802	501,1
13	1,25	1000	12160	460,3
14	1,25	1250	12261	474,5
15	1,25	1500	11073	430,5
16	1,00	750	12569	489,1
17	1,00	1000	11732	460,6
18	1,15	1000	11754	455,2
19	0,6	650	12579	488,5
20	0,5	600	12433	491,8

Examples of internal volumetric defect, called wormholes, were detected on the advancing side of some welds (see Fig. 5). In addition, on both side of welds, a rise of the stainless steel interface in the aluminum (called hooking) was frequently observed. This hooking reduces the effective thickness of the aluminum part and has a significant negative impact the tensile strength of the assembly. Adequate welding parameters can limit this phenomenon. The microstructure of a typical sound weld, considered to establish the process window, is presented in Fig. 6. In this weld, a small wormhole is visible on the retreating side and reduced hooking is observed on both side of the weld. These small defects have a limited impact on the tensile resistance of the assembly. For the weld presented in Fig. 6, a tensile shear resistance of 488 N/mm of weld is obtained. The lap shear samples almost all failed within the nugget of the aluminum alloy top sheet at the advancing side (see Fig. 7).

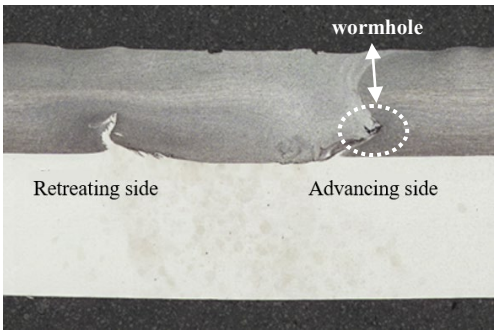

Figure 5. AA5083-H19/SS201LN ¼ hard lap weld, advancing speed = 1.25 m/min, rotational speed = 1500 RPM, axial force = 13 kN

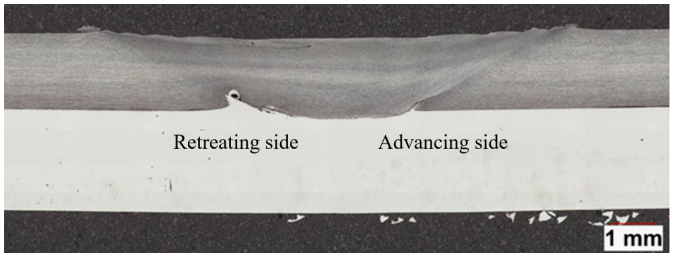

Figure 6. A5083-H19/SS201LN ¼ hard lap weld, advancing speed = 0.75 m/min, rotational speed = 750 RPM, axial force = 15 kN

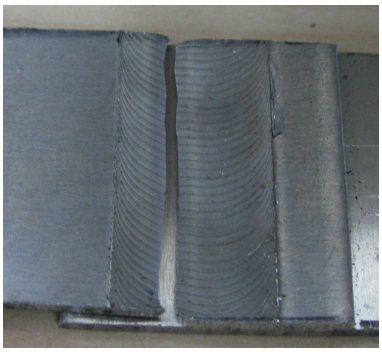

Figure 7. Lap shear fracture zone within FSW aluminium alloy weld nugget

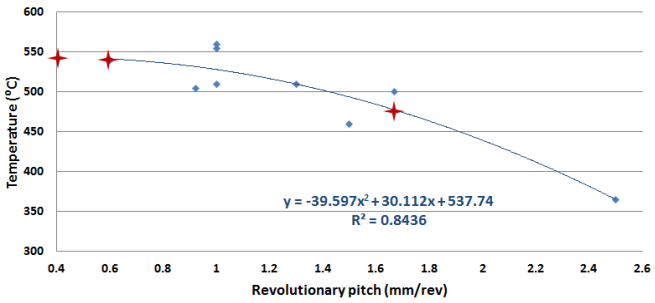

Figure 8. Weld temperature as function of the revolutionary pitch

The maximum weld temperatures, as function of the revolutionary pitch (travel speed / rotational speed) was determined for different sets of welding parameter and results are presented in Fig. 8. As illustrated, the weld temperature is function of the revolutionary pitch, which is an indication of the overall weld heat input. Globally, it is found that the lap shear strength is mainly function of the revolutionary pitch. Low heat input and colder welds favor higher strength.

Aluminum-steel intermetallic compounds were found at the weld interface and characterized by field-emission gun scanning electron microscopy (FEGSEM). Three different welding conditions, showing various degree of lap shear strength were chosen for this investigation (see Table V). The maximum temperature reached for these conditions are represented by red cross in Fig. 8.

TABLE V. WELDING CONDITIONS ANALYZED BY FEGSEM

Cond. #	Adv. Speed (m/min)	Rot. Speed (RPM)	Rev. pitch (mm/rev)	Approx. max weld temp. (°C)	Load/weld length (N/mm)
1	0.75	1250	0.60	542	416.2
2	0.30	750	0.40	543	442.1
3	1.25	750	1.67	478	501.0

For the first welding condition (cond. #1), a continuous intermetallic compound layer at the weld interface is observable. The intermetallic thickness lies between 1 and 4 µm (see Fig. 9). Based on electron discharge spectroscopy (EDS) analysis, the chemical composition of the intermetallic compounds promotes probable $Al_x(Fer_xMn_xCr_x)$ phase but further investigation in TEM would reveal the exact composition. The aluminum/iron chemical composition ratio is close to 2. The second welding condition (cond. #2) showed a completely different behavior (see Fig. 10). The intermetallic compound is much thicker, ranging from 7 to 15 µm, although the weld temperature is almost equivalent in comparison with cond. #1. The intermetallic growth is function of the maximum temperature but also the time spent at high temperature thus allowing diffusion. The lower travel speed of cond. #2 indicates a higher time spent at high temperature promoting the intermetallic growth observed. The chemical composition is very similar compare to the first condition.

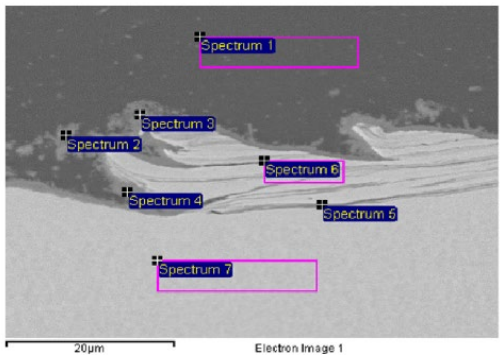

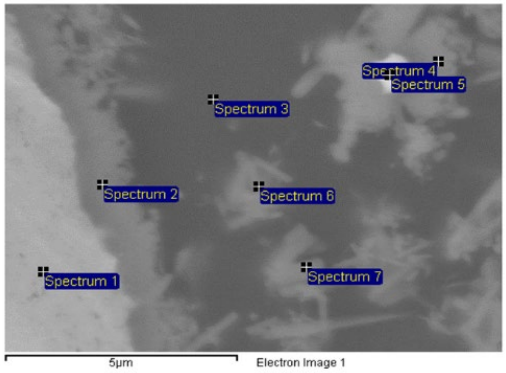

Spectrum	Mg	Al	Si	Cr	Mn	Fe	Ni	Total
Spectrum 1	0.39	18.31	0.44	13.36	6.28	57.64	3.59	100.00
Spectrum 2	1.76	59.76		5.67	2.94	28.25	1.63	100.00
Spectrum 3	5.38	93.29		0.56		0.78		100.00
Spectrum 4	2.53	65.93		4.13	2.60	22.92	1.90	100.00
Spectrum 5	0.74	20.33	0.56	12.13	5.61	56.88	3.76	100.00
Spectrum 6	4.75	75.87		6.77	3.03	9.58		100.00
Spectrum 7	6.21	79.17		5.57	2.81	6.24		100.00
Max.	6.21	93.29	0.56	13.36	6.28	57.64	3.76	
Min.	0.39	18.31	0.44	0.56	2.60	0.78	1.63	

Figure 9. Intermetallic compound found at aluminium-steel interface showed by FEGSEM; Cond. #1 (0.75 m/min, 1250RPM)

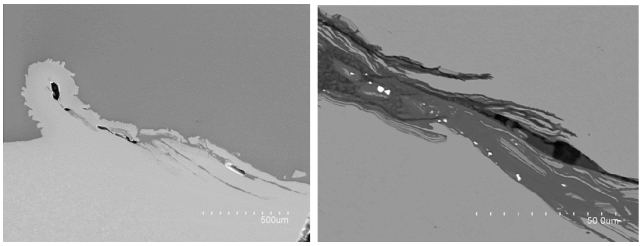

Figure 10. Intermetallic compound found at aluminium-steel interface showed by FEGSEM; Cond. #2 (0.3 m/min, 750RPM)

Finally, cond. #3, which shows the lowest temperature, dictates the thinnest intermetallic compounds (0.4-0.8 µm). The chemical composition is also different in comparison with the two welding conditions analyzed previously (Fig. 11). The iron content is higher indicating an aluminum/iron ratio close to 1.5 but with the same amount of manganese and chromium.

Spectrum	O	Mg	Al	Cr	Mn	Fe	Ni	Total
Spectrum 1		2.95	51.71	7.85	3.83	31.81	1.84	100.00
Spectrum 2		2.32	46.50	9.03	3.90	35.83	2.42	100.00
Spectrum 3		5.87	89.78	0.80	0.65	2.90		100.00
Spectrum 4	1.11	5.22	88.26	0.76	1.08	3.57		100.00
Spectrum 5	1.18	5.70	83.42	1.90	0.99	6.82		100.00
Max.	1.18	5.87	89.78	9.03	3.90	35.83	2.42	
Min.	1.11	2.32	46.50	0.76	0.65	2.90	1.84	

Figure 11. Intermetallic compound composition found at aluminium-steel interface showed by FEGSEM; Cond. #3 (1.25 m/min, 750RPM)

W and WC particles were also found on the advancing side of some welds. These particles can be seen in Fig. 10 and have the appearance of white spots in this figure.

Tool wear was investigated and tracked for two different welding conditions: 0.75 m/min at 750 RPM and 1.25 m/min at 1250 RPM. Wear was found to be predominant at the end of the pin tool, where the tool is in direct contact with the lower stainless steel part. At this location, stainless steel and aluminum layers stay attached to the tool after welding. To measure the effect of the wear on the pin length, the aluminum was removed from the tool with a 10% vol. NaOH solution. This procedure do not affect the tool geometry and stainless steel stay fixed to the tool. Fig. 12 shows a transversal view of a tool, after welding and cleaning. In this figure, the white line corresponds to the stainless steel, fixed to the tool during welding. Considering the presence of stainless steel on the pin tool and of tool particles in welds (W and WC), adhesive wear and abrasion are suspected to be dominant causes of tool deterioration. The evolution of tool wear was then evaluated after different welding lengths. Results presented in Figs. 13 and 14 show a linear relationship between the reduction of pin length and the welding length. For the two welding conditions tested, the wear rate is also similar and independent of the welding speed.

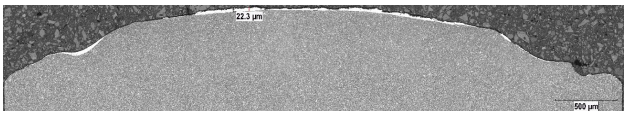

Figure 12. Transversal view of the pin tip, after welding

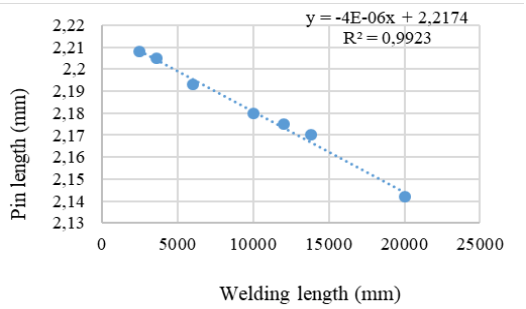

Figure 13. Evolution of pin length during welding at 0.75 m/min and 750 RPM

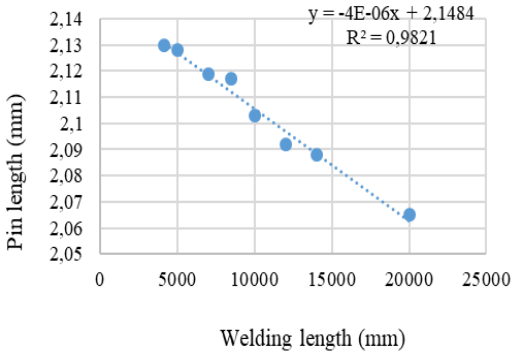

Figure 14. Evolution of pin length during welding at 1.25 m/min and 1250 RPM

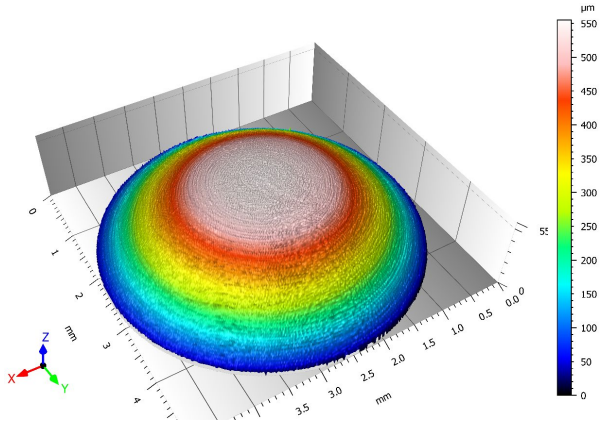

Figure 15. Microtopography of the tip of a new welding tool

The localization of the wear is also an important parameter to consider in tool life. To investigate the wear evolution, 3D pictures of the pin tool were done using microtopography and Mountain Maps software. The 3D geometry of the welding tool was analysed before and after welding. A 3D picture of a new pin tip is presented in Fig. 15 and have been compared with pictures of a tool, after 20 000 mm of weld made at 0.75 m/min and 750 rpm and at 1.25 m/min and 1250 rpm (respectively presented in Figs. 16 and 17). For the two conditions analyzed here, the wear is mainly located in the middle plane of the hemispherical plane. This wear produces a reduction of the tool radius. Moreover, the wear is more pronounced for the tool used at 1250 rpm. At this speed, the axial load is higher but the recorded torque applied on the tool is lower.

CONCLUSION

FSW can effectively produce lap joint between AA5083-H19 and SS201LN ¼ hard with tensile shear strength up to 500 N/mm of weld. In the welds produced, continuous intermetallic compound layers made of $Al_x(Fer_xMn_xCr_x)$ were observed at the interface between aluminum and stainless steel. Temperature and welding parameters influence the composition and the thickness of this layer.

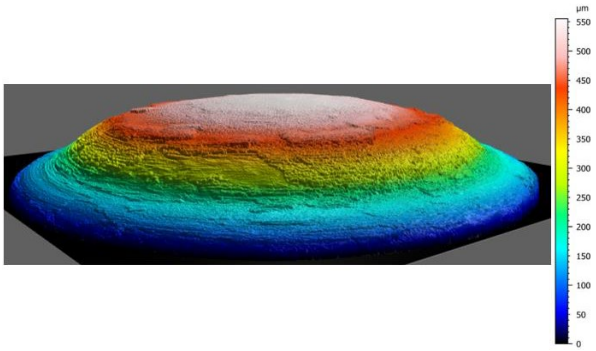

Figure 16. Microtopography of the tip of the welding tool used at 0.75 m/min and 750 rpm, after 20 000 mm of weld

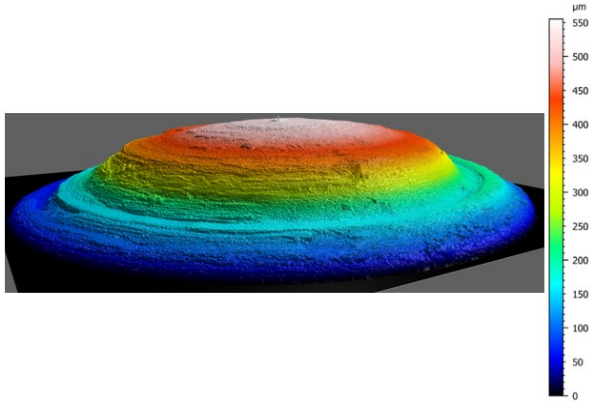

Figure 17. Microtopography of the tip of the welding tool used at 1.25 m/min and 1250 rpm, after 20 000 mm of weld

In addition, a significant degradation of the tool was observed. This wear was mainly located at the tip of the pin, where the tool is in direct contact with the stainless steel part. For the tested conditions, the wear rate is directly proportional to the length of the weld produced. Stainless steel attached to the tool after welding and WC particles found in welds suggest that abrasion and adhesion are present during the welding and were identified as dominant causes of wear.

REFERENCES

[1] L. St-Georges, L.I. Kiss, Friction Stir Welding: Principles and Applications, edited by the Presse de l'Aluminium, 2018.

[2] S. Ohhama, T. Hata, T. Yahaba, T. Kobayahsi et al., "Application of an FSW Continuous Welding Technology for Steel and Aluminum to an Automotive Subframe", SAE Technical Paper, 2013.

[3] S.A. Hussein, AS. Md Tahir, A.B. Hadzley, "Characteristics of aluminum-to-steel joint made by friction stirwelding: A review", Materials Today Communications 5, 2015, pp. 32-49.

[4] M. Santella, Y. Hovanski, T-Y Pan, "Friction Stir Spot Welding (FSSW) of Advanced High Strength Steels (AHSS)", SAE International 5(2), 2012, pp.382-387.

[5] W.J. Joost, "Reducing Vehicle Weight and Improving U.S. Energy Efficiency Using Integrated Computational Materials Engineering", JOM 64, 2012, pp.1032–1038.

[6] S. Argawal, P. E. Krajewski, and L. L. Briant, "Texture development and Dynamic Recrystallization in AA5083 during Superplastic Forming at Various Strain Rates", presented at the TMS, 2004.